Iranian Journal of Numerical Analysis and Optimization
Vol. ??, No. ??, ??, pp ??
https://doi.org/??
https://ijnao.um.ac.ir/

Research Article

Accurate ENO-like schemes for the model of fluid flows in a nozzle with variable cross-section

D.H. Cuong and M.D. Thanh*,

Abstract

A class of accurate high-order ENO-like schemes for the model of fluid flows in a nozzle with variable cross-section is presented. The model contains a nonconservative source term, which causes unsatisfactory results to standard numerical schemes, even for low-order ones. The proposed schemes rely on exact Riemann solvers and the reconstructed piecewise polynomials which are nonoscillatory. These schemes inherit the high-order precision of the ENO schemes like many existing ENO-type schemes, and possess a good accuracy. The ENO-like scheme corresponding to $k = 3$ can get the precision as good as van Leer-type schemes, and is numerically stable. Moreover, the ENO-like schemes for larger k may suffer from oscillations.

*Corresponding author

Received ??? ; revised ??? ; accepted ???

Dao Huy Cuong
Department of Mathematics, Ho Chi Minh City University of Education, Ho Chi Minh City, Vietnam. Email: cuongdh@hcmue.edu.vn

Mai Duc Thanh
Corresponding author, Department of Mathematics, International University, Ho Chi Minh City, Vietnam. Email: mdthanh@hcmiu.edu.vn
Vietnam National University, Ho Chi Minh City, Vietnam.

How to cite this article
Cuong, D.H. and Thanh, M.D., Accurate ENO-like schemes for the model of fluid flows in a nozzle with variable cross-section. *Iran. J. Numer. Anal. Optim.*, ??; ??(??): ??-??. ??

AMS subject classifications (2020): 65M08, 35L65, 76B15

Keywords: Nonconservative; Numerical approximation; Essentially nonoscillatory scheme; Accuracy; Resonance.

1 Introduction

Essentially nonoscillatory (ENO) schemes for hyperbolic conservation laws were first constructed by Harten et al. [24] in 1987. These high-resolution schemes have been developed by many authors for nonconservative systems, most use approximate Riemann solvers. In this paper, we aim to construct an ENO-like scheme relying on *exact Riemann solvers* for the following nonconservative system of balance laws, which models fluid flows in a nozzle with variable cross-section:

$$\begin{aligned} &\partial_t(a\rho) + \partial_x(a\rho u) = 0, \\ &\partial_t(a\rho u) + \partial_x(a(\rho u^2 + p)) = p\partial_x a, \quad x \in \mathbb{R}, \quad t > 0, \end{aligned} \tag{1}$$

where $\rho = \rho(x,t)$, $u = u(x,t)$, $p = p(x,t)$ denote the density, particle velocity, and pressure of the fluid, respectively, and $a = a(x)$ denotes the cross-section area of the nozzle.

The term $p\partial_x a$ on the right-hand side of the system (1) makes it nonconservative. Recall that the formulation of weak solutions of nonconservative systems of balance laws was introduced in [18]. Often, nonconservative terms cause unsatisfactory results for standard schemes. Therefore, numerical approximations of solutions of nonconservative systems of balance laws are one of the most challenging problems. Recently, we built a Godunov-type scheme for the model (1) in [15]. Our aim in this paper is to construct a high-resolution ENO-like scheme for (1). We will also demonstrate by numerical tests that the ENO-like scheme corresponding to $k = 3$ can provide us with a second order accurate approximation to a smooth stationary wave and a much better accuracy than the Godunov-type scheme. However, the ENO-like schemes for larger k may not be convergent, since oscillations can be observed.

For simplicity, we assume throughout that the fluid is isentropic and ideal, so that an equation of state is given by

$$p = \kappa \rho^{\gamma}, \tag{2}$$

where $\kappa > 0$ and $1 < \gamma < 5/3$ are constants.

Observe that there are many works in the literature about the study of nonconservative hyperbolic systems of balance laws. Basic theory of Riemann problem for models of fluid flows in a nozzle with discontinuous cross-section was considered in [25, 26, 32, 29, 38, 21]. In recent years, a related traffic flow model was formulated in [20], and a related model of shallow water flows over movable bottom with suspended and bedload transport was proposed in [8]. We refer the reader to the book [31] for the Riemann problem for various models in continuum physics. Regarding numerical methods, many results and schemes for models of fluid flows in a nozzle with variable cross-section were studied in [28, 27, 14, 5]. Recently, a second-order scheme based on the first-order Price-T scheme and the MUSCL-Hancock strategy for arterial blood flow models with viscoelasticity was constructed in [10]. Numerical schemes for the model of shallow water equations were studied in [22, 11, 30, 41]. Well-balanced finite difference WENO schemes using approximate solvers for the Ripa model were constructed in [23]. A set of arbitrarily high-order ENO-type schemes is constructed in a recent work [42] using a typical five-point smoothness measurement as the shock-detector, which are able to detect discontinuities before spatial reconstructions. Furthermore, ENO schemes with adaptive order which select a polynomial from several candidates that are reconstructed on stencils of unequal sizes are designed in [36]. A review on ENO schemes was given in [37]. Well-balanced numerical schemes for a single conservation law with source term were presented in

[6, 7, 3]. Numerical schemes for two-phase flow models were built in [4, 13, 12, 19, 1, 9, 33, 40, 39, 17]. The reader is referred to

[2, 34, 35] for Godunov-type schemes for hyperbolic systems of balance laws in nonconservative forms. See also the references therein.

The organization of this paper is as follows. Section 2 provides us with the background of the model (1). Section 3 is devoted to constructing an ENO-like scheme to calculate the approximate solution of the Cauchy problem for

(1). Numerical tests and discussions for all types of initial data are presented in Section 4. Finally, in section 5, we draw several conclusions.

2 Backgrounds

Let us set

$$c = \sqrt{dp/d\rho}.$$

Then the system (1) with supplementing a trivial equation

$$\partial_t a = 0, \tag{3}$$

can be rewritten in the nonconservative form as

$$\partial_t \mathbf{U} + \mathbf{A}(\mathbf{U})\partial_x \mathbf{U} = \mathbf{0}, \tag{4}$$

where

$$\mathbf{U} = \begin{bmatrix} \rho \\ u \\ a \end{bmatrix}, \quad \mathbf{A}(\mathbf{U}) = \begin{bmatrix} u & \rho & \rho u/a \\ c^2/\rho & u & 0 \\ 0 & 0 & 0 \end{bmatrix}.$$

The matrix $\mathbf{A}(\mathbf{U})$ has three eigenvalues

$$\lambda_1 = u - c, \quad \lambda_2 = u + c, \quad \lambda_3 = 0. \tag{5}$$

The corresponding eigenvectors can be chosen as

$$\mathbf{r}_1 = \begin{bmatrix} \rho \\ -c \\ 0 \end{bmatrix}, \quad \mathbf{r}_2 = \begin{bmatrix} \rho \\ c \\ 0 \end{bmatrix}, \quad \mathbf{r}_3 = \begin{bmatrix} -\rho u^2 \\ uc^2 \\ a(u^2 - c^2) \end{bmatrix}.$$

The first and the third characteristic speeds coincide on the *upper sonic surface*

$$\mathcal{C}^+ = \{\mathbf{U} | \lambda_1(\mathbf{U}) = \lambda_3(\mathbf{U})\}. \tag{6}$$

The second and the third characteristic speeds coincide on the *lower sonic surface*

$$\mathcal{C}^- = \{\mathbf{U} | \lambda_2(\mathbf{U}) = \lambda_3(\mathbf{U})\}. \tag{7}$$

Therefore, the system (4) is strictly hyperbolic on following regions:

$$G_1 = \{\mathbf{U}|\lambda_1(\mathbf{U}) > \lambda_3(\mathbf{U})\},$$
$$G_2 = \{\mathbf{U}|\lambda_1(\mathbf{U}) < \lambda_3(\mathbf{U}) < \lambda_2(\mathbf{U})\},$$
$$G_3 = \{\mathbf{U}|\lambda_2(\mathbf{U}) < \lambda_3(\mathbf{U})\}.$$

The set $G_1 \cup G_3$ is called the *supersonic region*, while G_2 is called the *subsonic region*. The third characteristic field is *linearly degenerate*, since

$$\nabla\lambda_3 \cdot \mathbf{r}_3 = 0.$$

The first and the second characteristic fields are *genuinely nonlinear*, since

$$-\nabla\lambda_1 \cdot \mathbf{r}_1 = \nabla\lambda_2 \cdot \mathbf{r}_2 = \frac{(\gamma+1)c}{2} > 0.$$

2.1 Shock wave curves

Recall that a *discontinuity wave* of (4) connecting a left-hand state $\mathbf{U}_-$ to a right-hand state $\mathbf{U}_+$ is a weak solution of the form

$$\mathbf{U}(x,t) = \begin{cases} \mathbf{U}_-, & \text{if } x < \sigma t, \\ \mathbf{U}_+, & \text{if } x > \sigma t, \end{cases} \tag{8}$$

where the speed of discontinuity wave σ must satisfy the Rankine–Hugoniot relations. The Rankine–Hugoniot relation associated with (3) takes the form

$$-\sigma[a] = 0, \tag{9}$$

where $[a] = a_+ - a_-$ denotes the jump of the quantity a. As discussed in [29], across a discontinuity wave there are two possibilities:

(i) either $[a] = 0$,

(ii) or $\sigma = 0$.

For the first case (i), a discontinuity wave (8) is called a *shock wave*. It called an i-Lax shock, if the shock speed $\sigma = \sigma_i(\mathbf{U}_-, \mathbf{U}_+)$ satisfies the Lax shock inequalities,

$$\lambda_i(\mathbf{U}_+) < \sigma_i(\mathbf{U}_-, \mathbf{U}_+) < \lambda_i(\mathbf{U}_-), \quad i = 1, 2.$$

Given a state $\mathbf{U}_0 = [\rho_0, u_0, a_0]^T$, the set of all right-hand states $\mathbf{U} = [\rho, u, a]^T$ that can be connected to $\mathbf{U}_0$ by a 1-Lax shock is given by

$$\mathcal{S}_1(\mathbf{U}_0) = \Big\{\mathbf{U} | u = u_0 - \sqrt{-(p-p_0)\Big(\frac{1}{\rho} - \frac{1}{\rho_0}\Big)}, \rho > \rho_0, a = a_0\Big\}, \tag{10}$$

and, in the backward way, the set of all left-hand states $\mathbf{U} = [\rho, u, a]^T$ that can be connected to $\mathbf{U}_0$ by a 2-Lax shock is given by

$$\mathcal{S}_{2B}(\mathbf{U}_0) = \Big\{\mathbf{U} | u = u_0 + \sqrt{-(p-p_0)\Big(\frac{1}{\rho} - \frac{1}{\rho_0}\Big)}, \rho > \rho_0, a = a_0\Big\}. \tag{11}$$

We call these set *the forward curve of* 1*-shock waves* and *the backward curve of* 1*-shock waves*, respectively.

Furthermore, we have the following result about the sign of the 1-shock speeds along the wave curve $\mathcal{S}_1(\mathbf{U}_0)$, which is shown in [29].

Lemma 1. If $\mathbf{U}_0 \in G_2 \cup G_3$, then $\sigma_1(\mathbf{U}_0, \mathbf{U})$ remains negative, that is,

$$\sigma_1(\mathbf{U}_0, \mathbf{U}) < 0, \quad \mathbf{U} \in \mathcal{S}_1(\mathbf{U}_0).$$

If $\mathbf{U}_0 \in G_1$, then there is exactly one state, denoted by $\mathbf{U}_0^\# = [\rho_0^\#, u_0^\#, a_0]^T \in \mathcal{S}_1(\mathbf{U}_0)$, such that

$$\begin{aligned}
&\mathbf{U}_0^\# \in G_2, \quad u_0^\# > 0,\\
&\sigma_1(\mathbf{U}_0, \mathbf{U}_0^\#) = 0,\\
&\sigma_1(\mathbf{U}_0, \mathbf{U}) > 0, \quad \rho_0 < \rho < \rho_0^\#,\\
&\sigma_1(\mathbf{U}_0, \mathbf{U}) < 0, \quad \rho > \rho_0^\#.
\end{aligned}$$

2.2 Stationary waves

For the case (ii), a discontinuity wave (8) is called a *stationary wave*, and the two states $\mathbf{U}_\pm$ are called the two *equilibrium states*. As shown in [29], two equilibrium states $\mathbf{U}_\pm$ must satisfy the jump relations

$$\begin{aligned}
&[a\rho u] = 0,\\
&\left[\frac{u^2}{2} + \frac{c^2}{\gamma - 1}\right] = 0.
\end{aligned} \tag{12}$$

Given the state $\mathbf{U}_0 = [\rho_0, u_0, a_0]^T$ and the cross-section level $a \neq a_0$. As discussed in [29], a stationary wave connecting from $\mathbf{U}_0$ to some state $\mathbf{U} = [\rho, u, a]^T$ exists if and only if $a \geq a_{\min}$, where

$$a_{\min} = \frac{a_0\rho_0|u_0|}{\sqrt{\kappa\gamma}(\rho_{\max})^{\frac{\gamma+1}{2}}}, \quad \rho_{\max} = \left(\frac{\gamma-1}{\kappa\gamma(\gamma+1)}\left(u_0^2 + \mu\rho_0^{\gamma-1}\right)\right)^{\frac{1}{\gamma-1}}. \tag{13}$$

Moreover, if $a > a_{\min}$, then there are exactly two states $\mathbf{U}_0^s$, $\mathbf{U}_0^b$ that can be connected to $\mathbf{U}_0$ by a stationary wave,

$$\begin{aligned} \mathbf{U}_0^s &= \left[\rho_0^s, \frac{a_0\rho_0u_0}{a\rho_0^s}, a\right]^T, \\ \mathbf{U}_0^b &= \left[\rho_0^b, \frac{a_0\rho_0u_0}{a\rho_0^b}, a\right]^T, \end{aligned} \tag{14}$$

where $\rho_0^s < \rho_{\max} < \rho_0^b$ are two roots of the nonlinear equation

$$-\frac{2\kappa\gamma}{\gamma-1}\mu\rho^{\gamma+1} + (u_0^2 + \frac{2\kappa\gamma}{\gamma-1}\rho_0^{\gamma-1})\rho^2 - (a_0u_0\rho_0/a)^2 = 0. \tag{15}$$

Precisely, we have the following lemma about stationary waves.

Lemma 2. [29, Lem. 2.3] The following conclusions hold:
a)

$$\begin{aligned} &\rho_{\max} > \rho_0, \quad \mathbf{U}_0 \in G_1 \cup G_3, \\ &\rho_{\max} < \rho_0, \quad \mathbf{U}_0 \in G_2, \\ &\rho_{\max} = \rho_0, \quad \mathbf{U}_0 \in \mathcal{C}^{\pm}. \end{aligned}$$

b) The state $\mathbf{U}_0^s$ belongs to G_1 if $u_0 > 0$, and belongs to G_3 if $u_0 < 0$, while the state $\mathbf{U}_0^b$ always belongs to G_2. In addition, it holds that

(i) If $a > a_0$, then

$$\rho_0^s < \rho_0 < \rho_0^b.$$

(ii) If $a < a_0$, then

$$\begin{aligned} &\rho_0 < \rho_0^s < \rho_0^b \quad \text{for} \quad \mathbf{U}_0 \in G_1 \cup G_3, \\ &\rho_0^s < \rho_0^b < \rho_0 \quad \text{for} \quad \mathbf{U}_0 \in G_2. \end{aligned}$$

It follows from Lemma 2 that there are two possible stationary waves from a given state $\mathbf{U}_0$ to a state with a new level cross-section a. Thus, it

is necessary to impose some condition to select a unique physical stationary state as follows.

(MC) Any stationary jump must not cross the sonic curve in the (ρ, u)-plane.

2.3 Rarefaction wave curves

Recall that the i-rarefaction wave ($i = 1, 2$) of (4) connecting a left-hand state $\mathbf{U}_-$ to a right-hand state $\mathbf{U}_+$ is a weak solution of the form

$$\mathbf{U}(x,t) = \begin{cases} \mathbf{U}_-, & \text{if } x < \lambda_i(\mathbf{U}_-)t, \\ \mathbf{V}_i(x/t), & \text{if } \lambda_i(\mathbf{U}_-)t \le x \le \lambda_i(\mathbf{U}_-)t, \\ \mathbf{U}_+, & \text{if } x > \lambda_i(\mathbf{U}_+)t, \end{cases}$$

where $\mathbf{V}_i(\cdot)$ is the solution of following problem:

$$\begin{aligned} &\frac{d\mathbf{V}_i(\xi)}{d\xi} = \frac{1}{\nabla\lambda_i(\mathbf{V}(\xi)) \cdot \mathbf{r}_i(\mathbf{V}(\xi))}\mathbf{r}_i(\mathbf{V}(\xi)), \quad \lambda_i(\mathbf{U}_-) < \xi < \lambda_i(\mathbf{U}_+), \\ &\mathbf{V}_i(\lambda_i(\mathbf{U}_-)) = \mathbf{U}_-, \quad \mathbf{V}_i(\lambda_i(\mathbf{U}_+)) = \mathbf{U}_+. \end{aligned}$$

Given a state $\mathbf{U}_0 = [\rho_0, u_0, a_0]^T$, the set of all right-hand states $\mathbf{U} = [\rho, u, a]^T$ that can be connected to U_0 by a 1-rarefaction wave forms *the forward curve of* 1*-rarefaction waves*, denoted by $\mathcal{R}_1(\mathbf{U}_0)$. In a backward way, the set of all left-hand states $\mathbf{U} = [\rho, u, a]^T$ that can be connected to $\mathbf{U}_0$ by a 2-rarefaction wave forms *the backward curve of* 2*-rarefaction wave*, denoted by $\mathcal{R}_{2B}(\mathbf{U}_0)$. These curves are given by

$$\begin{aligned} \mathcal{R}_1(\mathbf{U}_0) &= \Big\{\mathbf{U} | u = u_0 - \frac{2\sqrt{\kappa\gamma}}{\gamma - 1}(\rho^{(\gamma-1)/2} - \rho_0^{(\gamma-1)/2}), \rho \le \rho_0, a = a_0\Big\}, \\ \mathcal{R}_{2B}(\mathbf{U}_0) &= \Big\{\mathbf{U} | u = u_0 + \frac{2\sqrt{\kappa\gamma}}{\gamma - 1}(\rho^{(\gamma-1)/2} - \rho_0^{(\gamma-1)/2}), \rho \le \rho_0, a = a_0\Big\}. \end{aligned} \tag{16}$$

From (10), (11), and (16), we have the forward and backward wave curves in the nonlinear characteristic fields as follows:

$$\begin{aligned} \mathcal{W}_1(\mathbf{U}_0) &= \mathcal{R}_1(\mathbf{U}_0) \cup \mathcal{S}_1(\mathbf{U}_0), \\ \mathcal{W}_{2B}(\mathbf{U}_0) &= \mathcal{R}_{2B}(\mathbf{U}_0) \cup \mathcal{S}_{2B}(\mathbf{U}_0). \end{aligned} \tag{17}$$

2.4 Computing the Riemann solution

Observe that by the transformation $x \mapsto -x$, $u \mapsto -u$, a left-hand (right-hand) state $\mathbf{U} = [\rho, u, a]^T$ in G_2 (in G_3) will be transformed to the right-hand (left-hand, respectively) state $\mathbf{V} = [\rho, -u, a]^T$ in G_2 (in G_1, respectively). Therefore, the construction of the Riemann solutions for Riemann data around $\mathcal{C}^-$ can be obtained from the one for Riemann data around $\mathcal{C}^+$. Thus, without loss of generality, we consider only the case where Riemann data are in $G_1 \cup G_2$. We call construction A if $\mathbf{U}_L$ belongs to G_1, and construction B if $\mathbf{U}_L$ belongs to G_2. In each construction, we divide it into 3 cases depending on the relative position of the backward curve $\mathcal{W}_{2B}(\mathbf{U}_R)$ compared to the composite wave curves established in each construction.

In this subsection, we use some following notations:

(i) $W_k(\mathbf{U}_-, \mathbf{U}_+)$ ($S_k(\mathbf{U}_-, \mathbf{U}_+)$, $R_k(\mathbf{U}_-, \mathbf{U}_+)$) denotes the k-wave (k-shock, k-rarefaction wave, respectively) connecting the left-hand state $\mathbf{U}_-$ to the right-hand state $\mathbf{U}_+$, for $k = 1, 2, 3$.

(ii) $\mathbf{U}_0^{\#}$ denotes the state on the forward curve of 1-shock waves $\mathcal{S}_1(\mathbf{U}_0)$ such that $\sigma_1(U_0, U_0^{\#}) = 0$; see Lemma 1.

(iii) $\mathbf{U}_0^s, \mathbf{U}_0^b$ denote the states resulted by stationary contact wave from $\mathbf{U}_0$; see (14) and Lemma 2.

(iv) $\mathbf{U}_0^{\pm} = \mathcal{W}_1(\mathbf{U}_0) \cap \mathcal{C}^{\pm}$, where $\mathcal{W}_1(\mathbf{U}_0)$ is defined by (17) and $\mathcal{C}^{\pm}$ are defined by (6), (7).

(v) $\mathbf{U}^{\mathrm{Rie}}(x/t; \mathbf{U}_L, \mathbf{U}_R)$ is the exact solution of (4) with the Riemann initial data

$$\mathbf{U}(x, 0) = \begin{cases} \mathbf{U}_L, & \text{if } x < 0, \\ \mathbf{U}_R, & \text{if } x > 0. \end{cases} \tag{18}$$

2.4.1 Construction A1

Given a left-hand state $\mathbf{U}_L \in G_1$. If $\mathbf{U}_R$ is a state such that the backward curve $\mathcal{W}_{2B}(\mathbf{U}_R)$ intersects the composite wave curve $\mathcal{W}_3 \circ \mathcal{W}_1(\mathbf{U}_L, a_R)$, see

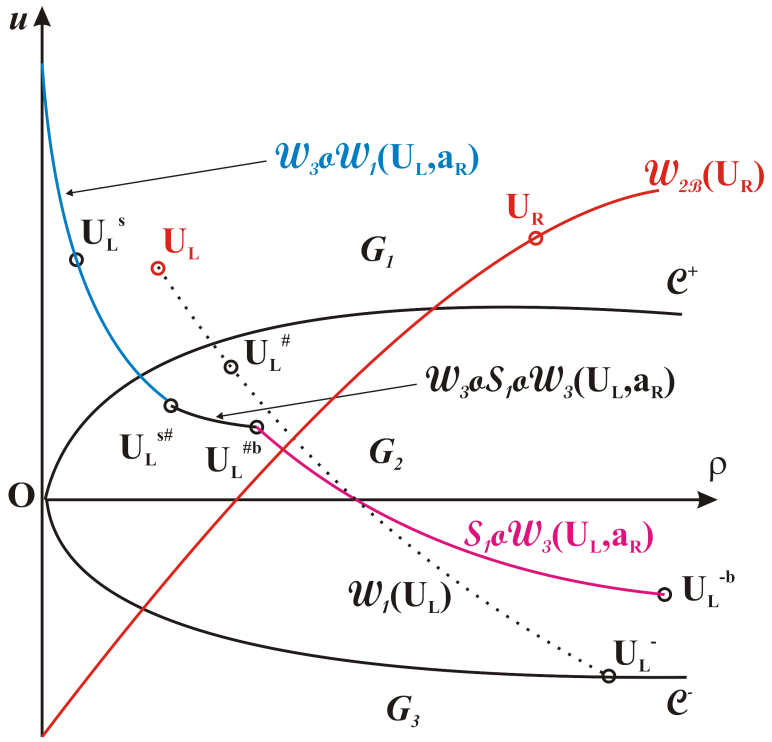

Figure 1: The composite wave curves $\mathcal{W}_3 \circ \mathcal{W}_1(\mathbf{U}_L, a_R)$, $\mathcal{W}_3 \circ \mathcal{S}_1 \circ \mathcal{W}_3(\mathbf{U}_L, a_R)$, $\mathcal{S}_1 \circ \mathcal{W}_3(\mathbf{U}_L, a_R)$, and the backward curve of 2-wave $\mathcal{W}_{2B}(\mathbf{U}_R)$

Figure 1, then the Riemann solution of (4) with initial data (18) is

$$\mathbf{U}^{\mathrm{Rie}}(x/t;\mathbf{U}_L,\mathbf{U}_R) \tag{19}$$
$$= \begin{cases} \mathbf{U}_L, & \text{if } x/t < 0, \\ \mathbf{U}_L^s, & \text{if } 0 < x/t < \min\{\lambda_1(\mathbf{U}_L^s), \lambda_1(\mathbf{U}_*)\}, \\ W_1(\mathbf{U}_L^s, \mathbf{U}_*), & \text{if } \min\{\lambda_1(\mathbf{U}_L^s), \lambda_1(\mathbf{U}_*)\} < x/t < \min\{\lambda_2(\mathbf{U}_*), \lambda_2(\mathbf{U}_R)\}, \\ W_2(\mathbf{U}_*, \mathbf{U}_R), & \text{if } x/t > \min\{\lambda_2(\mathbf{U}_*), \lambda_2(\mathbf{U}_R)\}, \end{cases}$$

where $\mathbf{U}_*$ is found by

$$\mathcal{W}_{2B}(\mathbf{U}_R) \cap \mathcal{W}_3 \circ \mathcal{W}_1(\mathbf{U}_L, a_R) = \{\mathbf{U}_*\},$$

with $\mathcal{W}_{2B}(\mathbf{U}_R)$ is defined by (17), and $\mathcal{W}_3 \circ \mathcal{W}_1(\mathbf{U}_L, a_R)$ is defined by

$$\mathcal{W}_3 \circ \mathcal{W}_1(\mathbf{U}_L, a_R) = \left\{ \mathbf{U} | \mathbf{U} \in \mathcal{W}_1(\mathbf{U}_L^s) \text{ and } \mathbf{U} \text{ is located above } \mathbf{U}_L^{s\#} \right\}. \tag{20}$$

The set $\mathcal{W}_3 \circ \mathcal{W}_1(\mathbf{U}_L, a_R)$ is called *the curve of composite* 3*-wave and* 1*-wave*, where $\mathbf{U}_L^s = \left[\rho_L^s, \dfrac{a_L \rho_L u_L}{a_R \rho_L^s}, a_R\right]^T$ is defined by Lemma 2, $\mathcal{W}_1(\mathbf{U}_L^s)$ is defined by (17), and $\mathbf{U}_L^{s\#} = \left(\mathbf{U}_L^s\right)^{\#}$ is defined by Lemma 1.

2.4.2 Construction A2

Given $\mathbf{U}_L \in G_1$. Whenever the backward curve $\mathcal{W}_{2B}(\mathbf{U}_R)$ intersects the composite wave curve $\mathcal{W}_3 \circ \mathcal{S}_1 \circ \mathcal{W}_3(\mathbf{U}_L, a_R)$, see Figure 1, the Riemann solution of (4) with initial data (18) is

$$\mathbf{U}^{\mathrm{Rie}}(x/t;\mathbf{U}_L,\mathbf{U}_R) = \begin{cases} \mathbf{U}_L, & \text{if } x/t < 0, \\ \mathbf{U}_*, & \text{if } 0 < x/t < \min\{\lambda_2(\mathbf{U}_*), \lambda_2(\mathbf{U}_R)\}, \\ W_2(\mathbf{U}_*, \mathbf{U}_R), & \text{if } x/t > \min\{\lambda_2(\mathbf{U}_*), \lambda_2(\mathbf{U}_R)\}, \end{cases} \tag{21}$$

where $\mathbf{U}_*$ is computed by

$$\mathcal{W}_{2B}(\mathbf{U}_R) \cap \mathcal{W}_3 \circ \mathcal{S}_1 \circ \mathcal{W}_3(\mathbf{U}_L, a_R) = \{\mathbf{U}_*\},$$

with $\mathcal{W}_{2B}(\mathbf{U}_R)$ is defined by (17), and $\mathcal{W}_3 \circ \mathcal{S}_1 \circ \mathcal{W}_3(\mathbf{U}_L, a_R)$ is defined by

$$\mathcal{W}_3 \circ \mathcal{S}_1 \circ \mathcal{W}_3(\mathbf{U}_L, a_R) = \Big\{ \mathbf{U}_L^{s\#b} | a_M \text{ is between } a_L \text{ and } a_R, \quad \mathbf{U}_L^s = \Big[\rho_L^s, \frac{a_L \rho_L u_L}{a_M \rho_L^s}, a_M\Big]^T, \quad \mathbf{U}_L^{s\#} = \Big(\mathbf{U}_L^s\Big)^{\#}, \quad \mathbf{U}_L^{s\#b} = \Big[(\rho_L^{s\#})^b, \frac{a_M \rho_L^{s\#} u_L^{s\#}}{a_R (\rho_L^{s\#})^b}, a_R\Big]^T \Big\}. \tag{22}$$

We call the set $\mathcal{W}_3 \circ \mathcal{S}_1 \circ \mathcal{W}_3(\mathbf{U}_L, a_R)$ *the curve of composite* 3*-wave,* 1*-shock, and* 3*-wave.*

2.4.3 Construction A3

Given $\mathbf{U}_L \in G_1$. If $\mathbf{U}_R$ is a state such that the backward curve $\mathcal{W}_{2B}(\mathbf{U}_R)$ intersects the composite wave curve $\mathcal{S}_1 \circ \mathcal{W}_3(\mathbf{U}_L, a_R)$ defined as below, see Figure 1, then the Riemann solution of (4) with initial data (18) is

$$\mathbf{U}^{\text{Rie}}(x/t; \mathbf{U}_L, \mathbf{U}_R) = \begin{cases} \mathbf{U}_L, & \text{if } x/t < \sigma_1(\mathbf{U}_L, \mathbf{U}_*), \\ \mathbf{U}_*, & \text{if } \sigma_1(\mathbf{U}_L, \mathbf{U}_*) < x/t < 0, \\ \mathbf{U}_*^b, & \text{if } 0 < x/t < \min\{\lambda_2(\mathbf{U}_*^b), \lambda_2(\mathbf{U}_R)\}, \\ W_2(\mathbf{U}_*^b, \mathbf{U}_R), & \text{if } x/t > \min\{\lambda_2(\mathbf{U}_*^b), \lambda_2(\mathbf{U}_R)\}, \end{cases} \tag{23}$$

where $\mathbf{U}_*$ and $\mathbf{U}_*^b$ are found by

$$\mathcal{W}_{2B}(\mathbf{U}_R) \cap \mathcal{S}_1 \circ \mathcal{W}_3(\mathbf{U}_L, a_R) = \{\mathbf{U}_*^b\},$$

with $\mathcal{W}_{2B}(\mathbf{U}_R)$ is defined by (17), and $\mathcal{S}_1 \circ \mathcal{W}_3(\mathbf{U}_L, a_R)$ is defined by

$$\mathcal{S}_1 \circ \mathcal{W}_3(\mathbf{U}_L, a_R) = \Big\{ \mathbf{U}_*^b | \mathbf{U}_* \in \mathcal{S}_1(\mathbf{U}_L), \mathbf{U}_* \text{ is located between } \mathbf{U}_L^{\#} \text{ and } \mathbf{U}_L^-, \quad \mathbf{U}_*^b = \Big[\rho_*^b, \frac{a_L \rho_* u_*}{a_R \rho_*^b}, a_R\Big]^T \Big\}. \tag{24}$$

The set $\mathcal{S}_1 \circ \mathcal{W}_3(\mathbf{U}_L, a_R)$ is called *the curve of composite* 1*-shock and* 3*-wave*, where $\mathcal{S}_1(\mathbf{U}_L)$ is defined by (10), $\mathbf{U}_L^{\#}$ is defined by Lemma 1, and $\mathbf{U}_L^- = \mathcal{S}_1(\mathbf{U}_L) \cap \mathcal{C}^-$.

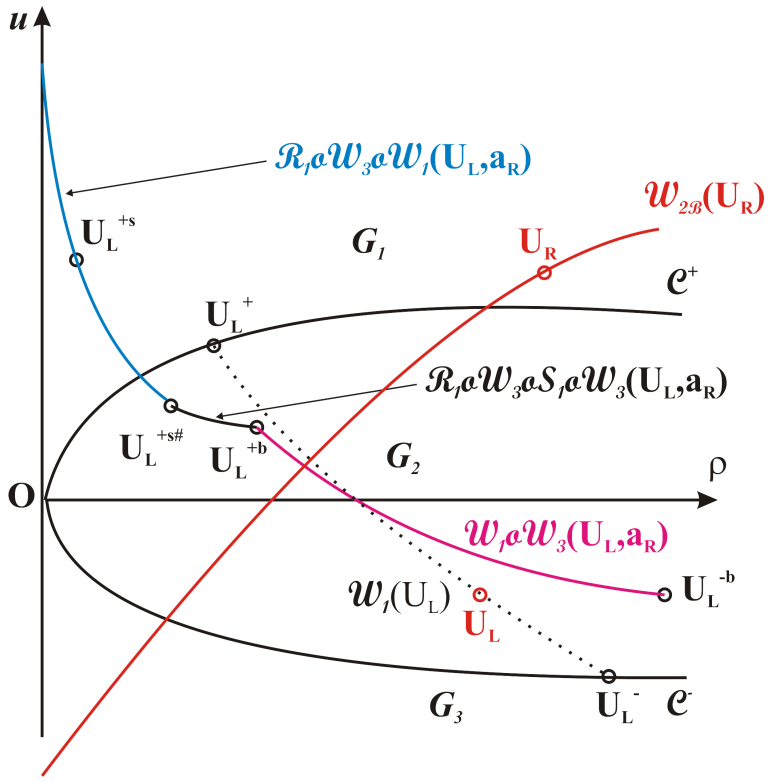

Figure 2: The composite wave curves $\mathcal{R}_1 \circ \mathcal{W}_3 \circ \mathcal{W}_1(\mathbf{U}_L, a_R)$, $\mathcal{R}_1 \circ \mathcal{W}_3 \circ \mathcal{S}_1 \circ \mathcal{W}_3(\mathbf{U}_L, a_R)$, $\mathcal{W}_1 \circ \mathcal{W}_3(\mathbf{U}_L, a_R)$, and the backward curve of 2-wave $\mathcal{W}_{2B}(\mathbf{U}_R)$

2.4.4 Construction B1

Given a left-hand state $\mathbf{U}_L \in G_2$. If a right-hand state $\mathbf{U}_R$ satisfies that the backward curve $\mathcal{W}_{2B}(\mathbf{U}_R)$ intersects the composite wave curve $\mathcal{R}_1 \circ \mathcal{W}_3 \circ \mathcal{W}_1(\mathbf{U}_L, a_R)$ defined as below, see Figure 2, then the Riemann solution of (4) with initial data (18) is

$$\mathbf{U}^{\mathrm{Rie}}(x/t; \mathbf{U}_L, \mathbf{U}_R) \tag{25}$$

$$= \begin{cases} R_1(\mathbf{U}_L, \mathbf{U}_L^+), & \text{if } x/t < 0, \\ \mathbf{U}_L^{+s}, & \text{if } 0 < x/t < \min\{\lambda_1(\mathbf{U}_L^{+s}), \lambda_1(\mathbf{U}_*)\}, \\ W_1(\mathbf{U}_L^{+s}, \mathbf{U}_*), & \text{if } \min\{\lambda_1(\mathbf{U}_L^{+s}), \lambda_1(\mathbf{U}_*)\} < x/t < \min\{\lambda_2(\mathbf{U}_*), \lambda_2(\mathbf{U}_R)\}, \\ W_2(\mathbf{U}_*, \mathbf{U}_R), & \text{if } x/t > \min\{\lambda_2(\mathbf{U}_*), \lambda_2(\mathbf{U}_R)\}, \end{cases}$$

where $\mathbf{U}_*$ is found by

$$\mathcal{W}_{2B}(\mathbf{U}_R) \cap \mathcal{R}_1 \circ \mathcal{W}_3 \circ \mathcal{W}_1(\mathbf{U}_L, a_R) = \{\mathbf{U}_*\},$$

with $\mathcal{W}_{2B}(\mathbf{U}_R)$ is defined by (17), and $\mathcal{R}_1 \circ \mathcal{W}_3 \circ \mathcal{W}_1(\mathbf{U}_L, a_R)$ is defined by

$$\mathcal{R}_1 \circ \mathcal{W}_3 \circ \mathcal{W}_1(\mathbf{U}_L, a_R) = \left\{\mathbf{U} | \mathbf{U} \in \mathcal{W}_1(\mathbf{U}_L^{+s}) \text{ and } \mathbf{U} \text{ is located above } \mathbf{U}_L^{+s\#}\right\}. \tag{26}$$

The set $\mathcal{R}_1 \circ \mathcal{W}_3 \circ \mathcal{W}_1(\mathbf{U}_L, a_R)$ is called *the curve of composite* 1*-rarefaction wave,* 3*-wave, and* 1*-wave*, where $\mathbf{U}_L^+ = \mathcal{R}_1(\mathbf{U}_L) \cap \mathcal{C}^+$, $\mathbf{U}_L^{+s} = \left[(\rho_L^+)^s, \dfrac{a_L \rho_L^+ u_L^+}{a_R (\rho_L^+)^s}, a_R\right]^T$ is defined by Lemma 2, $\mathcal{R}_1(\mathbf{U}_L)$ and $\mathcal{W}_1(\mathbf{U}_L^{+s})$ are defined by (16), (17), and $\mathbf{U}_L^{+s\#} = \left(\mathbf{U}_L^{+s}\right)^{\#}$ is defined by Lemma 1.

2.4.5 Construction B2

Given a left-hand state $\mathbf{U}_L \in G_2$. Whenever the backward curve $\mathcal{W}_{2B}(\mathbf{U}_R)$ intersects the composite wave curve $\mathcal{R}_1 \circ \mathcal{W}_3 \circ \mathcal{S}_1 \circ \mathcal{W}_3(\mathbf{U}_L, a_R)$, see Figure 2, the Riemann solution of (4) with initial data (18) will be

$$\mathbf{U}^{\text{Rie}}(x/t; \mathbf{U}_L, \mathbf{U}_R) = \begin{cases} R_1(\mathbf{U}_L, \mathbf{U}_L^+), & \text{if } x/t < 0, \\ \mathbf{U}_*, & \text{if } 0 < x/t < \min\{\lambda_2(\mathbf{U}_*), \lambda_2(\mathbf{U}_R)\}, \\ W_2(\mathbf{U}_*, \mathbf{U}_R), & \text{if } x/t > \min\{\lambda_2(\mathbf{U}_*), \lambda_2(\mathbf{U}_R)\}, \end{cases} \tag{27}$$

where $\mathbf{U}_*$ is calculated by

$$\mathcal{W}_{2B}(\mathbf{U}_R) \cap \mathcal{R}_1 \circ \mathcal{W}_3 \circ \mathcal{S}_1 \circ \mathcal{W}_3(\mathbf{U}_L, a_R) = \{\mathbf{U}_*\},$$

with $\mathcal{W}_{2B}(\mathbf{U}_R)$ is defined by (17), and $\mathcal{R}_1 \circ \mathcal{W}_3 \circ \mathcal{S}_1 \circ \mathcal{W}_3(\mathbf{U}_L, a_R)$ is defined by

$$\mathcal{R}_1\circ\mathcal{W}_3\circ\mathcal{S}_1\circ\mathcal{W}_3(\mathbf{U}_L,a_R)=\Big\{\mathbf{U}_L^{+s\#b}|a_M \text{ is between } a_L \text{ and } a_R,\\ \mathbf{U}_L^{+s}=\Big[(\rho_L^+)^s,\frac{a_L\rho_L^+u_L^+}{a_M(\rho_L^+)^s},a_M\Big]^T,\\ \mathbf{U}_L^{+s\#}=\Big(\mathbf{U}_L^{+s}\Big)^{\#},\\ \mathbf{U}_L^{+s\#b}=\Big[(\rho_L^{+s\#})^b,\frac{a_M\rho_L^{+s\#}u_L^{+s\#}}{a_R(\rho_L^{+s\#})^b},a_R\Big]^T\Big\}. \tag{28}$$

We refer the set $\mathcal{R}_1\circ\mathcal{W}_3\circ\mathcal{S}_1\circ\mathcal{W}_3(\mathbf{U}_L,a_R)$ as *the curve of composite* 1*-rarefaction wave,* 3*-wave,* 1*-shock, and* 3*-wave*, where $\mathbf{U}_L^+=\mathcal{R}_1(\mathbf{U}_L)\cap\mathcal{C}^+$.

2.4.6 Construction B3

Given a left-hand state $\mathbf{U}_L\in G_2$. If $\mathbf{U}_R$ is a right-hand state such that the backward curve $\mathcal{W}_{2B}(\mathbf{U}_R)$ intersects the composite wave curve $\mathcal{W}_1\circ\mathcal{W}_3(\mathbf{U}_L,a_R)$, see Figure 2, then the Riemann solution of (4) with initial data (18) is

$$\mathbf{U}^{\mathrm{Rie}}(x/t;\mathbf{U}_L,\mathbf{U}_R)=\begin{cases}W_1(\mathbf{U}_L,\mathbf{U}_*), & \text{if } x/t<0,\\ \mathbf{U}_*^b, & \text{if } 0<x/t<\min\{\lambda_2(\mathbf{U}_*^b),\lambda_2(\mathbf{U}_R)\},\\ W_2(\mathbf{U}_*^b,\mathbf{U}_R), & \text{if } x/t>\min\{\lambda_2(\mathbf{U}_*^b),\lambda_2(\mathbf{U}_R)\},\end{cases} \tag{29}$$

where $\mathbf{U}_*$ and $\mathbf{U}_*^b$ are found by

$$\mathcal{W}_{2B}(\mathbf{U}_R)\cap\mathcal{W}_1\circ\mathcal{W}_3(\mathbf{U}_L,a_R)=\{\mathbf{U}_*^b\},$$

with $\mathcal{W}_{2B}(\mathbf{U}_R)$ is defined by (17), and $\mathcal{W}_1\circ\mathcal{W}_3(\mathbf{U}_L,a_R)$ is defined by

$$\mathcal{W}_1\circ\mathcal{W}_3(\mathbf{U}_L,a_R)=\Big\{\mathbf{U}_*^b|\mathbf{U}_*\in\mathcal{W}_1(\mathbf{U}_L),\mathbf{U}_* \text{ is located between } \mathbf{U}_L^+ \text{ and } \mathbf{U}_L^-,\\ \mathbf{U}_*^b=\Big[\rho_*^b,\frac{a_L\rho_*u_*}{a_R\rho_*^b},a_R\Big]^T\Big\}. \tag{30}$$

The set $\mathcal{W}_1\circ\mathcal{W}_3(\mathbf{U}_L,a_R)$ is called *the curve of composite* 1*-wave and* 3*-wave*, where $\mathcal{W}_1(\mathbf{U}_L)$ is defined by (17), and $\mathbf{U}_L^{\pm}=\mathcal{W}_1(\mathbf{U}_L)\cap\mathcal{C}^{\pm}$.

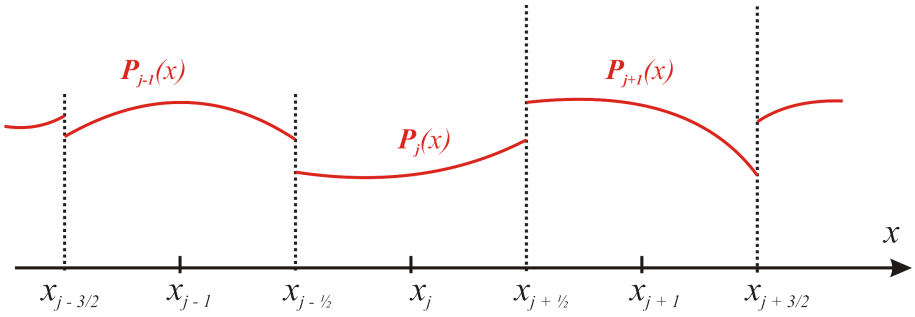

Figure 3: The piecewise polynomial $\mathbf{U}_{\text{p.pol}}(x)$

3 Building an ENO-type scheme

Relying on the constructions of Riemann solutions in the previous section, we are now in a position to construct an ENO-type scheme for (4). Let us set

$$\mathbf{U} = \begin{bmatrix} a\rho \\ a\rho u \\ a \end{bmatrix}, \quad \mathbf{F}(\mathbf{U}) = \begin{bmatrix} a\rho u \\ a(\rho u^2 + p) \\ 0 \end{bmatrix}, \quad \mathbf{H}(\mathbf{U}) = \begin{bmatrix} 0 \\ p \\ 0 \end{bmatrix}. \tag{31}$$

Then, the system (4) can be written in form

$$\partial_t \mathbf{U} + \partial_x \mathbf{F}(\mathbf{U}) = \mathbf{H}(\mathbf{U})\partial_x a, \quad x \in \mathbb{R}, \quad t > 0. \tag{32}$$

Given the initial condition

$$\mathbf{U}(x,0) = \mathbf{U}_0(x), \quad x \in \mathbb{R}, \tag{33}$$

we define the discrete initial values $\{\mathbf{U}_j^0\}_{j\in\mathbb{Z}}$ are given by

$$\mathbf{U}_j^0 = \frac{1}{\Delta x}\int_{x_{j-1/2}}^{x_{j+1/2}} \mathbf{U}_0(x)dx, \quad j \in \mathbb{Z}. \tag{34}$$

Suppose that the approximation $\{\mathbf{U}_j^n\}_{j\in\mathbb{Z}}$ of $\mathbf{U}$ at the time t_n is known. Recently, the Godunov-type scheme is built in [15] as

$$\mathbf{U}_j^{n+1} = \mathbf{U}_j^n - \frac{\Delta t}{\Delta x}\Big(\mathbf{F}(\mathbf{U}^{\text{Rie}}(0-;\mathbf{U}_j^n,\mathbf{U}_{j+1}^n)) - \mathbf{F}(\mathbf{U}^{\text{Rie}}(0+;\mathbf{U}_{j-1}^n,\mathbf{U}_j^n))\Big), \tag{35}$$

where Δt must satisfy the C.F.L condition

$$\frac{\Delta t}{\Delta x}\max\{|\lambda_i(\mathbf{U}_j^n)| : j\in\mathbb{Z}, i=1,2\}\le \text{CFL}. \tag{36}$$

Then, the van Leer-type scheme is built in [16] as

$$\mathbf{U}_j^{n+1} = \mathbf{U}_j^n - \frac{\Delta t}{\Delta x}\Big(\mathbf{F}(\mathbf{U}^{\text{Rie}}(0-;\mathbf{U}_{j+1/2,-}^{n+1/2},\mathbf{U}_{j+1/2,+}^{n+1/2})) \tag{37}$$

$$-\mathbf{F}(\mathbf{U}^{\text{Rie}}(0+;\mathbf{U}_{j-1/2,-}^{n+1/2},\mathbf{U}_{j-1/2,+}^{n+1/2}))\Big), \tag{38}$$

where

$$\begin{aligned}
\mathbf{U}_{j+1/2,-}^{n+1/2} &= \mathbf{U}_{j+1/2,-}^{n} - \frac{\Delta t}{2\Delta x}(\mathbf{F}(\mathbf{U}_{j+1/2,-}^{n}) - \mathbf{F}(\mathbf{U}_{j-1/2,+}^{n})),\\
\mathbf{U}_{j-1/2,+}^{n+1/2} &= \mathbf{U}_{j-1/2,+}^{n} - \frac{\Delta t}{2\Delta x}(\mathbf{F}(\mathbf{U}_{j+1/2,-}^{n}) - \mathbf{F}(\mathbf{U}_{j-1/2,+}^{n})),\\
\mathbf{U}_{j+1/2,-}^{n} &= \mathbf{U}_{j}^{n} + \frac{1}{2}\mathbf{S}_j^n,\\
\mathbf{U}_{j-1/2,+}^{n} &= \mathbf{U}_{j}^{n} - \frac{1}{2}\mathbf{S}_j^n,\\
\mathbf{S}_j^n &= (\mathbf{U}_{j+1}^n - \mathbf{U}_j^n)\Phi(\theta_j^n),\\
\theta_j^n &= \frac{\mathbf{U}_j^n - \mathbf{U}_{j-1}^n}{\mathbf{U}_{j+1}^n - \mathbf{U}_j^n},\\
\Phi(\theta) &= \frac{|\theta|+\theta}{1+|\theta|}.
\end{aligned}$$

Now, in this paper, we construct an ENO-type scheme as follows:

(1) From the sequence $\mathbf{U}^n$, we construct a piecewise polynomial $\mathbf{U}_{\text{p.pol}}(\cdot)$ as follows:

$$\mathbf{U}_{\text{p.pol}}(x) = \mathbf{P}_j(x) = \begin{bmatrix}\rho_j(x)\\ u_j(x)\\ a_j(x)\end{bmatrix}, \quad x_{j-1/2}<x<x_{j+1/2}, \quad j\in\mathbb{Z}, \tag{39}$$

where for each j, $\mathbf{P}_j(x)$ is a polynomial of degree at most $k-1$, and there exist $r,s\in\mathbb{N}$ (depending on j) such that

$$\begin{aligned}
&\frac{1}{\Delta x}\int_{x_{i-1/2}}^{x_{i+1/2}}\mathbf{P}_j(x)dx = \mathbf{U}_i^n, \quad i\in\{j-r,\dots,j,\dots,j+s\},\\
&s+r+1=k;
\end{aligned} \tag{40}$$

see Figure 3. For each j, to achieve the polynomial $\mathbf{P}_j(x)$ satisfying (40), we first look for the primitive function $\mathbf{Q}_j(x)$ of $\mathbf{P}_j(x)$, that is,

$$\mathbf{Q}_j(x) = \int_{-\infty}^{x} \mathbf{P}_j(x)dx,$$

in the following way:

(i) We start with the two node stencil for $\mathbf{Q}_j(x)$

$$\{x_{j-1/2}, x_{j+1/2}\},$$

and compute the first order divided difference

$$\mathbf{Q}_j[x_{j-1/2}, x_{j+1/2}] = \frac{\mathbf{Q}_j(x_{j+1/2}) - \mathbf{Q}_j(x_{j-1/2})}{\Delta x},$$

where

$$\mathbf{Q}_j(x_{j+1/2}) = \sum_{l=-\infty}^{j} \mathbf{U}_l^n \Delta x,$$
$$\mathbf{Q}_j(x_{j-1/2}) = \sum_{l=-\infty}^{j-1} \mathbf{U}_l^n \Delta x.$$

(ii) Assume that l-node stencil for $\mathbf{Q}_j(x)$ $(l = 2, 3, \ldots, k)$

$$\{x_{i+1/2}, \ldots, x_{i+l-1/2}\}$$

is known. To add one of two neighboring nodes, $x_{i-1/2}$ or $x_{i+l+1/2}$, to the stencil, we use the following ENO procedure:

* If

$$\Big|\mathbf{Q}_j[x_{i-1/2}, x_{i+1/2}, \ldots, x_{i+l-1/2}]\Big| < \Big|\mathbf{Q}_j[x_{i+1/2}, \ldots, x_{i+l-1/2}, x_{i+l+1/2}]\Big|,$$

then we add $x_{i-1/2}$ to the stencil, where the lth order divided differences are defined recursively by

$$\mathbf{Q}_j[x_{i+1/2}, \ldots, x_{i+l+1/2}] = \frac{\mathbf{Q}_j[x_{i+3/2}, \ldots, x_{i+l+1/2}] - \mathbf{Q}_j[x_{i+1/2}, \ldots, x_{i+l-1/2}]}{l\Delta x};$$

* Otherwise, we add $x_{i+l+1/2}$ to the stencil.

(iii) After the $(k+1)$-node stencil

$$\{x_{j-r-1/2}, x_{j-r+1/2}, \ldots, x_{j-1/2}, x_{j+1/2}, \ldots, x_{j+s-1/2}, x_{j+s+1/2}\},$$

is found, where $s + r + 1 = k$, we use Newton interpolation formula to obtain $\mathbf{Q}_j(x)$, which is a polynomial of degree at most k, satisfying

$$\mathbf{Q}_j(x_{i+1/2}) = \sum_{l=-\infty}^{i} \mathbf{U}_l^n \Delta x, \quad i = j - r - 1, \ldots, j + s.$$

Then, we obtain

$$\mathbf{P}_j(x) = \frac{d}{dx}\mathbf{Q}_j(x),$$

which is a polynomial of degree at most $k-1$ satisfying (40).

(2) We solve the Cauchy problem for (32) with the initial condition

$$\mathbf{U}(x, 0) = \mathbf{U}_{\text{p.pol}}(x), \quad x \in \mathbb{R}, \tag{41}$$

to find the solution $\mathbf{U}(\cdot, \Delta t)$.

(3) We project $\mathbf{U}(\cdot, \Delta t)$ onto the piecewise constant functions, that is, we set

$$\mathbf{U}_j^{n+1} = \frac{1}{\Delta x} \int_{x_{j-1/2}}^{x_{j+1/2}} \mathbf{U}(x, \Delta t) dx, \quad j \in \mathbb{Z}. \tag{42}$$

In order to obtain an explicit scheme, we integrate the equation (32) over the rectangle $(x_{j-1/2}, x_{j+1/2}) \times (0, \Delta t)$, we obtain

$$\begin{aligned} &\int_{x_{j-1/2}}^{x_{j+1/2}} (\mathbf{U}(x, \Delta t) - \mathbf{U}(x, 0)) dx \\ &+ \int_0^{\Delta t} \Big(\mathbf{F}(\mathbf{U}(x_{j+1/2} - 0, t)) - \mathbf{F}(\mathbf{U}(x_{j-1/2} + 0, t))\Big) dt \\ &\quad = \int_{x_{j-1/2}}^{x_{j+1/2}} \int_0^{\Delta t} \mathbf{H}(\mathbf{U}) \partial_x a dt dx. \end{aligned} \tag{43}$$

Using (40), (39), (41) and (42), we get

$$\begin{aligned} &\Delta x(\mathbf{U}_j^{n+1} - \mathbf{U}_j^n) + \int_0^{\Delta t} \Big(\mathbf{F}(\mathbf{U}(x_{j+1/2} - 0, t)) - \mathbf{F}(\mathbf{U}(x_{j-1/2} + 0, t))\Big) dt \\ &= \int_{x_{j-1/2}}^{x_{j+1/2}} \int_0^{\Delta t} \mathbf{H}(\mathbf{U}(x, t)) \partial_x a_j(x) dt dx. \end{aligned} \tag{44}$$

Approximating (44) by using the Midpoint Rule, we obtain

$$\begin{aligned}&\Delta x(\mathbf{U}_j^{n+1}-\mathbf{U}_j^n)+\Delta t\Big(\mathbf{F}(\mathbf{U}(x_{j+1/2}-0,\Delta t/2))-\mathbf{F}(\mathbf{U}(x_{j-1/2}+0,\Delta t/2))\Big)dt\\&=\Delta x\Delta t\mathbf{H}(\mathbf{U}(x_j,\Delta t/2))\cdot\partial_x a_j(x)\Big|_{x=x_j}.\end{aligned}\tag{45}$$

To approximate $\mathbf{F}(\mathbf{U}(x_{j+1/2}-0,\Delta t/2))$, $\mathbf{F}(\mathbf{U}(x_{j-1/2}+0,\Delta t/2))$, and $\mathbf{H}(\mathbf{U}(x_j,\Delta t/2))$, we use a predictor-corrector method as follows:

(i) We compute the updated values $\mathbf{U}_{j+1/2,\pm}^{n+1/2}$ by

$$\begin{aligned}&\mathbf{U}_{j+1/2,-}^{n+1/2}\\&=\mathbf{U}_{j+1/2,-}^{n}-\frac{\Delta t}{2\Delta x}(\mathbf{F}(\mathbf{U}_{j+1/2,-}^{n})-\mathbf{F}(\mathbf{U}_{j-1/2,+}^{n}))\\&\quad+\frac{\Delta t}{2}\mathbf{H}(\mathbf{U}_{j+1/2,-}^{n})\cdot\partial_x a_j(x)\Big|_{x=x_{j+1/2}-},\\&\mathbf{U}_{j-1/2,+}^{n+1/2}\\&=\mathbf{U}_{j-1/2,+}^{n}-\frac{\Delta t}{2\Delta x}(\mathbf{F}(\mathbf{U}_{j+1/2,-}^{n})-\mathbf{F}(\mathbf{U}_{j-1/2,+}^{n}))\\&\quad+\frac{\Delta t}{2}\mathbf{H}(\mathbf{U}_{j-1/2,+}^{n})\cdot\partial_x a_j(x)\Big|_{x=x_{j-1/2}+},\end{aligned}\tag{46}$$

where

$$\begin{aligned}\mathbf{U}_{j+1/2,-}^{n}&=\mathbf{P}_j(x_{j+1/2}),\\\mathbf{U}_{j-1/2,+}^{n}&=\mathbf{P}_j(x_{j-1/2}).\end{aligned}\tag{47}$$

(ii) We solve the Riemann problem of (32) with initial data

$$\mathbf{U}(x,0)=\begin{cases}\mathbf{U}_{j+1/2,-}^{n+1/2},\text{if } x<x_{j+1/2},\\\mathbf{U}_{j+1/2,+}^{n+1/2},\text{if } x>x_{j+1/2},\end{cases}\qquad x_j<x<x_{j+1},\quad j\in\mathbb{Z},\tag{48}$$

to obtain the exact solution

$$\mathbf{U}(x,t)=\mathbf{U}^{\mathrm{Rie}}\Big(\frac{x-x_{j+1/2}}{t};\mathbf{U}_{j+1/2,-}^{n+1/2},\mathbf{U}_{j+1/2,+}^{n+1/2}\Big),\quad x_j<x<x_{j+1},\quad j\in\mathbb{Z}.\tag{49}$$

(iii) We approximate

$$\begin{aligned}
\mathbf{F}(\mathbf{U}(x_{j+1/2}-0,\Delta t/2)) \approx& \mathbf{F}(\mathbf{U}^{\mathrm{Rie}}(0-;\mathbf{U}^{n+1/2}_{j+1/2,-},\mathbf{U}^{n+1/2}_{j+1/2,+})),\\
\mathbf{F}(\mathbf{U}(x_{j-1/2}+0,\Delta t/2)) \approx& \mathbf{F}(\mathbf{U}^{\mathrm{Rie}}(0+;\mathbf{U}^{n+1/2}_{j-1/2,-},\mathbf{U}^{n+1/2}_{j-1/2,+})),\\
\mathbf{H}(\mathbf{U}(x_j,\Delta t/2)) \approx& \frac{1}{2}\Big(\mathbf{H}(\mathbf{U}^{\mathrm{Rie}}(0-;\mathbf{U}^{n+1/2}_{j+1/2,-},\mathbf{U}^{n+1/2}_{j+1/2,+}))\\
&+\mathbf{H}(\mathbf{U}^{\mathrm{Rie}}(0+;\mathbf{U}^{n+1/2}_{j-1/2,-},\mathbf{U}^{n+1/2}_{j-1/2,+}))\Big).
\end{aligned}$$

Thus, the scheme (45) becomes

$$\begin{aligned}
\mathbf{U}^{n+1}_j =& \mathbf{U}^n_j - \frac{\Delta t}{\Delta x}\Big(\mathbf{F}(\mathbf{U}^{\mathrm{Rie}}(0-;\mathbf{U}^{n+1/2}_{j+1/2,-},\mathbf{U}^{n+1/2}_{j+1/2,+}))\\
&-\mathbf{F}(\mathbf{U}^{\mathrm{Rie}}(0+;\mathbf{U}^{n+1/2}_{j-1/2,-},\mathbf{U}^{n+1/2}_{j-1/2,+}))\Big)\\
&+\frac{\Delta t}{2}\Big(\mathbf{H}(\mathbf{U}^{\mathrm{Rie}}(0-;\mathbf{U}^{n+1/2}_{j+1/2,-},\mathbf{U}^{n+1/2}_{j+1/2,+}))\\
&+\mathbf{H}(\mathbf{U}^{\mathrm{Rie}}(0+;\mathbf{U}^{n+1/2}_{j-1/2,-},\mathbf{U}^{n+1/2}_{j-1/2,+}))\Big)\cdot \partial_x a_j(x)\Big|_{x=x_j}.
\end{aligned} \tag{50}$$

To complete the ENO-type scheme (50), we must visit the Riemann problem for (1) to define the values $\mathbf{U}^{\mathrm{Rie}}(0\pm;\mathbf{U}_L,\mathbf{U}_R)$ as follows:

- For construction A1 (19): $\mathbf{U}^{\mathrm{Rie}}(0-;\mathbf{U}_L,\mathbf{U}_R)=\mathbf{U}_L$, and $\mathbf{U}^{\mathrm{Rie}}(0+;\mathbf{U}_L,\mathbf{U}_R)=\mathbf{U}^s_L$, where $\mathbf{U}^s_L=\left[\rho^s_L,\dfrac{a_L\rho_L u_L}{a_R\rho^s_L},a_R\right]^T$ is defined by Lemma 2.

- For construction A2 (21): $\mathbf{U}^{\mathrm{Rie}}(0-;\mathbf{U}_L,\mathbf{U}_R)=\mathbf{U}_L$, and $\mathbf{U}^{\mathrm{Rie}}(0+;\mathbf{U}_L,\mathbf{U}_R)=\mathbf{U}_*$, where $\mathbf{U}_*$ is the intersection point of $\mathcal{W}_{2B}(\mathbf{U}_R)$ defined by (17), and $\mathcal{W}_3\circ\mathcal{S}_1\circ\mathcal{W}_3(\mathbf{U}_L,a_R)$ defined by (22).

- For construction A3 (23): $\mathbf{U}^{\mathrm{Rie}}(0-;\mathbf{U}_L,\mathbf{U}_R)=\mathbf{U}_*$, and $\mathbf{U}^{\mathrm{Rie}}(0+;\mathbf{U}_L,\mathbf{U}_R)=\mathbf{U}^b_*$, where $\mathbf{U}_*$ belongs to $\mathcal{S}_1(\mathbf{U}_L)$ defined by (10), and $\mathbf{U}^b_*$ is the intersection point of $\mathcal{W}_{2B}(\mathbf{U}_R)$ defined by (17), and $\mathcal{S}_1\circ\mathcal{W}_3(\mathbf{U}_L,a_R)$ defined by (24).

- For construction B1 (25): $\mathbf{U}^{\mathrm{Rie}}(0-;\mathbf{U}_L,\mathbf{U}_R)=\mathbf{U}^+_L$, and $\mathbf{U}^{\mathrm{Rie}}(0+;\mathbf{U}_L,\mathbf{U}_R)=\mathbf{U}^{+s}_L$, where $\mathbf{U}^+_L=\mathcal{R}_1(\mathbf{U}_L)\cap\mathcal{C}^+$, and $\mathbf{U}^{+s}_L=\left[(\rho^+_L)^s,\dfrac{a_L\rho^+_L u^+_L}{a_R(\rho^+_L)^s},a_R\right]^T$ is defined by Lemma 2.

- For construction B2 (27): $\mathbf{U}^{\mathrm{Rie}}(0-;\mathbf{U}_L,\mathbf{U}_R)=\mathbf{U}^+_L$, and $\mathbf{U}^{\mathrm{Rie}}(0+;\mathbf{U}_L,\mathbf{U}_R)=\mathbf{U}_*$, where $\mathbf{U}_*$ is the intersection point of $\mathcal{W}_{2B}(\mathbf{U}_R)$ defined by (17), and $\mathcal{R}_1\circ\mathcal{W}_3\circ\mathcal{S}_1\circ\mathcal{W}_3(\mathbf{U}_L,a_R)$ defined by (28).

- For construction B3 (29): $\mathbf{U}^{\mathrm{Rie}}(0-;\mathbf{U}_L,\mathbf{U}_R)=\mathbf{U}_*$, and $\mathbf{U}^{\mathrm{Rie}}(0+;\mathbf{U}_L,\mathbf{U}_R)=\mathbf{U}_*^b$, where $\mathbf{U}_*$ belongs to $\mathcal{W}_1(\mathbf{U}_L)$ defined by (17), and $\mathbf{U}_*^b$ is the intersection point of $\mathcal{W}_{2B}(\mathbf{U}_R)$ defined by (17), and $\mathcal{W}_1\circ\mathcal{W}_3(\mathbf{U}_L,a_R)$ defined by (30).

4 Numerical experiments with discussions

This section is aimed to demonstrate the accuracy of our scheme (50) with some numerical tests with MATLAB. For each test, we find the numerical solutions $\mathbf{U}_h$ by our scheme (50) with taking

$$\kappa=1.0,\quad \gamma=1.6,$$

and we then compare $\mathbf{U}_h$ with the corresponding exact solution $\mathbf{U}$.

4.1 Test for well-balanced property

Test 1. In this test, we aim to demonstrate that the ENO-like scheme (50) can capture a smooth stationary wave with second order accuracy. Let us consider the Cauchy problem for system (4) with the initial smooth data given by

$$\mathbf{U}(x,0)=\Big[\rho(x),u(x),a(x)\Big]^T,\quad x\geq 0, \tag{51}$$

where $a(x)=1+\dfrac{1}{2}x^3$, and $\Big(\rho(\cdot),u(\cdot)\Big)$ is the solution of the following problem:

$$\begin{aligned}
&\frac{d}{dx}(a\rho u)=0,\\
&\frac{d}{dx}\Big(\frac{u^2}{2}+\frac{\kappa\gamma\rho^{\gamma-1}}{\gamma-1}\Big)=0,\\
&(\rho,u)\Big|_{x=0}=(0.5,1.5),\\
&\lambda_1(\rho,u)=u-\sqrt{\kappa\gamma\rho^{\gamma-1}}>0,\quad x\geq 0.
\end{aligned} \tag{52}$$

The exact solution of this problem is just a smooth stationary wave

$$\mathbf{U}(x,t)=\Big[\rho(x),u(x),a(x)\Big]^T,\quad x\geq 0,\quad t\geq 0.$$

Figure 4 displays the exact solution and the approximate solution by the ENO-like scheme (50) with $k = 3$ for the mesh size $h = 1/80$ at time $t = 0.1$ and on spatial domain $x \in [0, 1]$. The errors, orders of convergence are reported by Table 1.

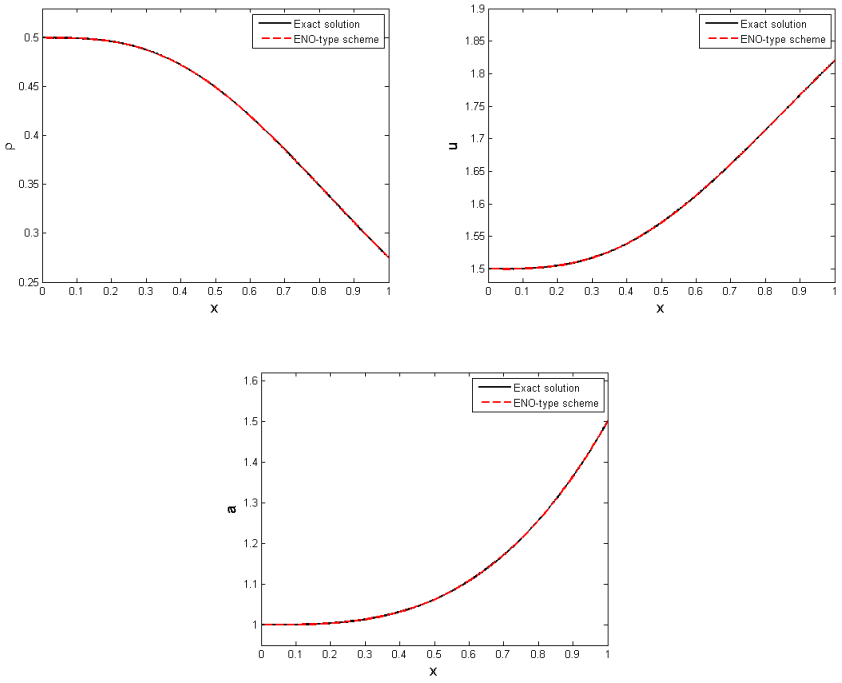

Figure 4: Exact solution and approximate solution by the ENO-like scheme (50) with $k = 3$ for the mesh size $h = 1/80$ at time $t = 0.1$ and on spatial domain $x \in [0, 1]$ of Test 1

4.2 Test for a complete Riemann solution when initial data belongs to same region

Test 2. In this test, we approximate the Riemann solution of the problem (4) with initial data

Table 1: Errors and orders of convergence for Test 1

h	L^1-error	Order
1/10	0.20912×10^{-3}	–
1/20	0.05769×10^{-3}	1.86
1/40	0.013918×10^{-3}	2.05
1/80	0.003443×10^{-3}	2.02
1/160	0.000917×10^{-3}	1.91

$$\begin{array}{c|c|c} & \mathbf{U}_L & \mathbf{U}_R \\ \hline \rho & 0.5 & 0.7 \\ \hline u & 1.5 & 2.0 \\ \hline a & 2.0 & 2.5 \end{array} \tag{53}$$

where $\mathbf{U}_L, \mathbf{U}_R$ are in the same supersonic region G_1. According to the Construction A1, the Riemann solution is

$$\mathbf{U}(x,t) = \begin{cases} \mathbf{U}_L, & \text{if } x/t < 0, \\ \mathbf{U}_L^s, & \text{if } 0 < x/t < \sigma_1(\mathbf{U}_L^s, \mathbf{U}_*), \\ \mathbf{U}_*, & \text{if } \sigma_1(\mathbf{U}_L^s, \mathbf{U}_*) < x/t < \lambda_2(\mathbf{U}_*), \\ R_2(\mathbf{U}_*, \mathbf{U}_R), & \text{if } x/t > \lambda_2(\mathbf{U}_*), \end{cases}$$

where

	$\mathbf{U}_L^s$	$\mathbf{U}_*$
ρ	0.350918	0.436769
u	1.709803	1.50012
a	2.5	2.5

Figure 5 displays the exact solution and its approximate solutions by the ENO-like scheme (50) with $k = 3$ and $k = 7$ for the mesh size $h = 1/320$ at time $t = 0.1$ and on spatial domain $x \in [-1, 1]$. The errors, orders of convergence are reported in Table 2. This table shows that the errors of the ENO-like scheme (50) are much smaller than the ones of the Godunov-type scheme (35), and the orders of convergence of the ENO-like scheme (50) are higher than the ones of the Godunov-type scheme (35) for all $k =$

$2, 3, 4, 5, 6, 7$. Specially, the errors of the ENO-like scheme (50) with $k = 3$ are smaller than the ones of the van Leer-type scheme (38), although very small.

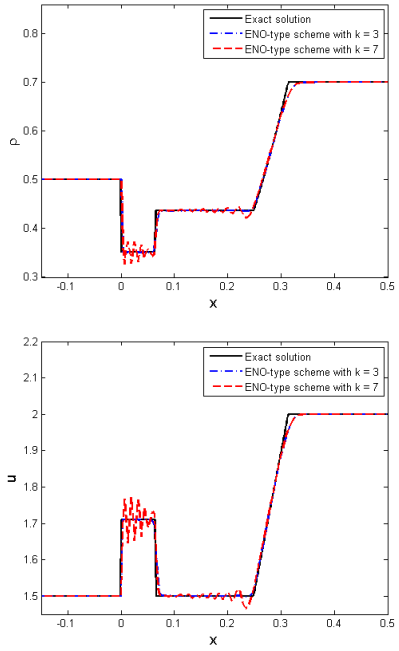

Figure 5: Exact solution and its approximate solutions by the ENO-like scheme (50) with $k = 3$ and $k = 7$ for the mesh size $h = 1/320$ at time $t = 0.1$ of Test 2

4.3 Test for a complete Riemann solution when initial data belongs to different regions

Test 3. Consider the Riemann data

	$\mathbf{U}_L$	$\mathbf{U}_R$
ρ	0.9	0.5
u	1.0	1.2
a	2.0	2.5

(54)

Table 2: Errors and orders of convergence for Test 2

	Godunov-type		van Leer-type		ENO-like $k=2$		ENO-like $k=3$	
h	L^1-error	Order	L^1-error	Order	L^1-error	Order	L^1-error	Order
1/10	0.147210	–	0.133470	–	0.137800	–	0.136490	–
1/20	0.092721	0.67	0.071526	0.90	0.075273	0.87	0.070917	0.94
1/40	0.056977	0.70	0.037260	0.94	0.039782	0.92	0.035419	1.00
1/80	0.036229	0.65	0.017500	1.09	0.020400	0.96	0.016978	1.06
1/160	0.023050	0.65	0.008817	0.99	0.010675	0.93	0.008495	1.00
1/320	0.014581	0.66	0.004534	0.96	0.005647	0.92	0.004427	0.94
	ENO-like $k=4$		ENO-like $k=5$		ENO-like $k=6$		ENO-like $k=7$	
h	L^1-error	Order	L^1-error	Order	L^1-error	Order	L^1-error	Order
1/10	0.138800	–	0.141660	–	0.144350	–	0.135280	–
1/20	0.072094	0.95	0.074614	0.92	0.076848	0.91	0.072276	0.90
1/40	0.034414	1.07	0.035282	1.08	0.036509	1.07	0.036410	0.99
1/80	0.016349	1.07	0.016685	1.08	0.017567	1.06	0.019454	0.90
1/160	0.008891	0.88	0.009398	0.83	0.011317	0.63	0.012965	0.59
1/320	0.004822	0.88	0.005238	0.84	0.006964	0.70	0.007721	0.75

where $\mathbf{U}_L \in G_2$, and $\mathbf{U}_R \in G_1$. According to the Construction B1, the exact solution is

$$\mathbf{U}(x,t) = \begin{cases} R_1(\mathbf{U}_L, \mathbf{U}_L^+), & \text{if } x/t < 0, \\ \mathbf{U}_L^{+s}, & \text{if } 0 < x/t < \sigma_1(\mathbf{U}_L^{+s}, \mathbf{U}_*), \\ \mathbf{U}_*, & \text{if } \sigma_1(\mathbf{U}_L^{+s}, \mathbf{U}_*) < x/t < \sigma_2(\mathbf{U}_*, \mathbf{U}_R), \\ \mathbf{U}_R, & \text{if } x/t > \sigma_2(\mathbf{U}_*, \mathbf{U}_R), \end{cases}$$

where

	$\mathbf{U}_L^+$	$\mathbf{U}_L^{+s}$	$\mathbf{U}_*$
ρ	0.778780	0.446692	0.582528
u	1.173504	1.636746	1.360876
a	2.0	2.5	2.5

Figure 6 displays the exact solution and its approximate solutions by the ENO-like scheme (50) with $k = 3$ and $k = 6$ for the mesh size $h = 1/320$ at time $t = 0.1$ and on spatial domain $x \in [-1, 1]$. The errors, orders of convergence are reported in Table 3. This test indicates that the errors of the ENO-like scheme (50) are smaller than those of the Godunov-type scheme

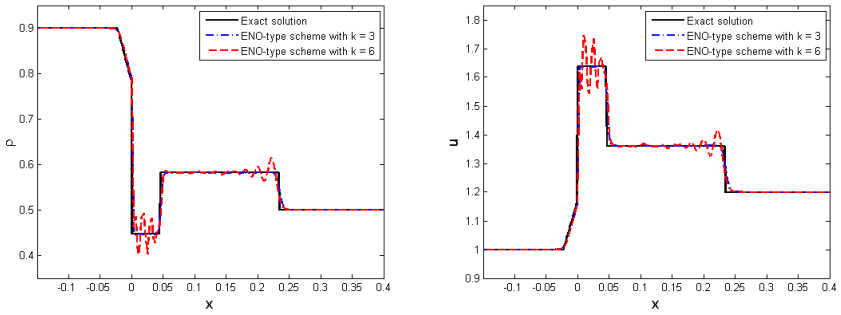

Figure 6: Exact solution and approximate solutions by the ENO-like scheme (50) with $k = 3$ and $k = 6$ for the mesh size $h = 1/320$ at time $t = 0.1$ of Test 3

(35) only for $k = 2, 3, 4$. Specially, the errors, orders of convergence of the ENO-like scheme (50) with $k = 3$ are approximate to the ones of the van Leer-type scheme (38).

Table 3: Errors and orders of convergence for Test 3

	Godunov-type		van Leer-type		ENO-like $k = 2$		ENO-like $k = 3$	
h	L^1-error	Order	L^1-error	Order	L^1-error	Order	L^1-error	Order
1/10	0.145170	–	0.140000	–	0.143600	–	0.141710	–
1/20	0.088237	0.72	0.083727	0.74	0.085501	0.75	0.085796	0.72
1/40	0.045084	0.97	0.038502	1.12	0.038707	1.14	0.039072	1.13
1/80	0.026477	0.77	0.019911	0.95	0.020432	0.92	0.020352	0.94
1/160	0.015181	0.80	0.009689	1.04	0.010287	0.99	0.009670	1.07
1/320	0.009123	0.73	0.005674	0.77	0.005962	0.79	0.005467	0.82
	ENO-like $k = 4$		ENO-like $k = 5$		ENO-like $k = 6$		ENO-like $k = 7$	
h	L^1-error	Order	L^1-error	Order	L^1-error	Order	L^1-error	Order
1/10	0.141280	–	0.141260	–	0.141420	–	0.141640	–
1/20	0.086031	0.72	0.086124	0.71	0.086201	0.71	0.086289	0.71
1/40	0.040304	1.09	0.041208	1.06	0.041770	1.05	0.042117	1.03
1/80	0.023236	0.79	0.025029	0.72	0.026564	0.65	0.027639	0.61
1/160	0.011882	0.97	0.015186	0.72	0.017823	0.58	0.019678	0.49
1/320	0.006408	0.89	0.009008	0.75	0.010765	0.73	0.013075	0.59

4.4 Test for a resonant phenomenon case

Test 4. This test is conducted to show that the scheme (50) can work well in regions of resonance, where three waves propagate at same speed. Consider the Riemann initial data

	$\mathbf{U}_L$	$\mathbf{U}_R$
ρ	0.5	1.2
u	1.5	0.9
a	2.0	2.5

(55)

where $\mathbf{U}_L \in G_1$, and $\mathbf{U}_R \in G_2$. According to the Construction A2, the exact solution is

$$\mathbf{U}(x,t) = \begin{cases} \mathbf{U}_L & \text{if } x/t < 0, \\ \mathbf{U}_L^{s\#b}, & \text{if } 0 < x/t < \lambda_2(\mathbf{U}_L^{s\#b}), \\ R_2(\mathbf{U}_L^{s\#b}, \mathbf{U}_R), & \text{if } x/t > \lambda_2(\mathbf{U}_L^{s\#b}), \end{cases} \tag{56}$$

where

	$\mathbf{U}_L^s$	$\mathbf{U}_L^{s\#}$	$\mathbf{U}_L^{s\#b}$
ρ	0.458944	0.886495	0.966873
u	1.557664	0.806412	0.620557
a	2.098252	2.098252	2.5

In this Riemann solution (56), we can see that it contains three waves propagating at zero speed, that is, $W_3(\mathbf{U}_L, \mathbf{U}_L^s)$, $S_1(\mathbf{U}_L^s, \mathbf{U}_L^{s\#})$, and $W_3(\mathbf{U}_L^{s\#}, \mathbf{U}_L^{s\#b})$.

Figure 7 shows the exact solution and its approximate solutions by the ENO-like scheme (50) with $k = 3$ and $k = 5$ for the mesh size $h = 1/320$ at time $t = 0.1$ and on spatial domain $x \in [-1, 1]$. This figure demonstrates the convergence of the approximate solutions by the ENO-like scheme (50) when the Riemann data belongs to regions of resonance. The errors, orders of convergence are reported in Table 4. We can see from this table that the ENO-like scheme (50) with $k = 2, 3, 4, 5, 6$ has a better accuracy than the Godunov-type scheme (35). Again, we also see that the errors, orders of convergence of the ENO-like scheme (50) with $k = 3$ are the same as those of the van Leer-type scheme (38).

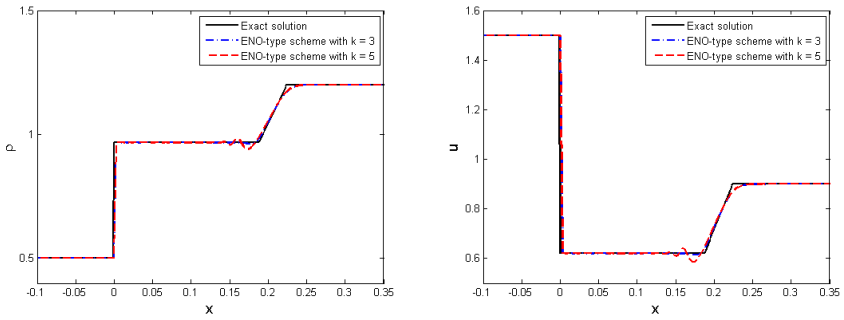

Figure 7: Exact solution and approximate solutions by the ENO-like scheme (50) with $k = 3$ and $k = 5$ for the mesh size $h = 1/320$ at the time $t = 0.1$ of Test 4

Table 4: Errors and orders of convergence for Test 4

	Godunov-type		van Leer-type		ENO-like $k = 2$		ENO-like $k = 3$	
h	L^1-error	Order	L^1-error	Order	L^1-error	Order	L^1-error	Order
1/10	0.156310	–	0.149430	–	0.146500	–	0.147310	–
1/20	0.089646	0.80	0.078463	0.93	0.078737	0.90	0.076385	0.95
1/40	0.053216	0.75	0.042118	0.90	0.043172	0.87	0.042851	0.83
1/80	0.030277	0.81	0.021359	0.98	0.022269	0.96	0.021173	1.02
1/160	0.017451	0.79	0.010617	1.01	0.011415	0.96	0.010297	1.04
1/320	0.010445	0.74	0.005360	0.99	0.005884	0.96	0.005193	0.99
	ENO-like $k = 4$		ENO-like $k = 5$		ENO-like $k = 6$		ENO-like $k = 7$	
h	L^1-error	Order	L^1-error	Order	L^1-error	Order	L^1-error	Order
1/10	0.147400	–	0.147240	–	0.147090	–	0.147890	–
1/20	0.076007	0.96	0.076504	0.94	0.076737	0.94	0.080435	0.88
1/40	0.044977	0.76	0.046037	0.73	0.046879	0.71	0.049658	0.70
1/80	0.023064	0.96	0.024237	0.93	0.025491	0.88	0.030240	0.72
1/160	0.011652	0.99	0.012472	0.96	0.013368	0.93	0.025279	0.26
1/320	0.006026	0.95	0.006472	0.95	0.007058	0.92	0.018523	0.45

4.5 Test for interaction of waves

Test 5. In this test, we approximate a Cauchy problem with initial condition:

$$\mathbf{U}(x,0) = \begin{cases} \mathbf{U}_L = [0.8, 2.0, 2.0]^T, & \text{if } x < 0, \\ \mathbf{U}_M = [0.5, 1.5, 2.5]^T, & \text{if } 0 < x < 1, \\ \mathbf{U}_R = [0.372067, 1.679806, 3.0]^T, & \text{if } x > 1, \end{cases} \tag{57}$$

where $\mathbf{U}_L, \mathbf{U}_M, \mathbf{U}_R \in G_1$, and $\mathbf{U}_R = \mathbf{U}_M^s$. At time $t = 0.4$, we can check that the Riemann solution at $x = 0$ interacts with the one at $x = 1$. Therefore, the exact solution at $t = 0.4$ is

$$\mathbf{U}(x,t) = \begin{cases} \mathbf{U}_L, & \text{if } x/t < 0, \\ \mathbf{U}_1, & \text{if } 0 < x/t < \sigma_1(\mathbf{U}_1, \mathbf{U}_2), \\ \mathbf{U}_2, & \text{if } \sigma_1(\mathbf{U}_1, \mathbf{U}_2) < x/t \text{ and } (x-1)/t < 0, \\ \mathbf{U}_3, & \text{if } 0 < (x-1)/t < \sigma_1(\mathbf{U}_3, \mathbf{U}_4), \\ \mathbf{U}_4, & \text{if } \sigma_1(\mathbf{U}_3, \mathbf{U}_4) < (x-1)/t < \sigma_2(\mathbf{U}_4, \mathbf{U}_R), \\ \mathbf{U}_R, & \text{if } (x-1)/t > \sigma_2(\mathbf{U}_4, \mathbf{U}_R), \end{cases}$$

where

	$\mathbf{U}_1$	$\mathbf{U}_2$	$\mathbf{U}_3$	$\mathbf{U}_4$
ρ	0.584096	0.738236	0.567757	0.562968
u	2.191420	1.929233	2.090433	2.099463
a	2.5	2.5	3.0	3.0

Figure 8 displays the exact solution and its approximate solutions by the ENO-like scheme (50) with $k = 3$ and $k = 5$ for the mesh size $h = 1/320$ at time $t = 0.4$ and on spatial domain $x \in [-2, 2]$. The errors, orders of convergence are reported in Table 5. Like all tests above, this test also indicates that the errors of the ENO-like scheme (50) with $k = 2, 3, 4, 5$ are much smaller than the ones of the Godunov-type scheme (35), and the orders of convergence of the ENO-like scheme (50) with $k = 2, 3, 4, 5$ are higher than the ones of the Godunov-type scheme (35). We also see that the accuracy of the ENO-like scheme (50) is less than the van Leer-type scheme (38) for all $k = 2, 3, 4, 5, 6, 7$.

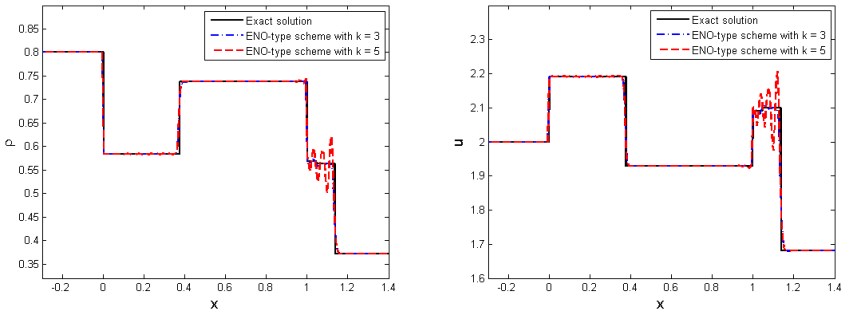

Figure 8: Exact solution and approximate solutions by the ENO-like scheme (50) with $k = 3$ and $k = 5$ for the mesh size $h = 1/160$ at time $t = 0.4$ of Test 5

Table 5: Errors and orders of convergence for Test 5

	Godunov-type		van Leer-type		ENO-like $k = 2$		ENO-like $k = 3$	
h	L^1-error	Order	L^1-error	Order	L^1-error	Order	L^1-error	Order
1/5	0.218000	–	0.164300	–	0.180440	–	0.170460	–
1/10	0.161200	0.44	0.095635	0.78	0.112080	0.69	0.102300	0.74
1/20	0.107390	0.59	0.045529	1.07	0.057382	0.97	0.052002	0.98
1/40	0.067436	0.67	0.024359	0.90	0.029569	0.96	0.026578	0.97
1/80	0.041364	0.71	0.011765	1.05	0.015053	0.97	0.012180	1.13
1/160	0.023396	0.82	0.005772	1.03	0.007526	1.00	0.006322	0.95
	ENO-like $k = 4$		ENO-like $k = 5$		ENO-like $k = 6$		ENO-like $k = 7$	
h	L^1-error	Order	L^1-error	Order	L^1-error	Order	L^1-error	Order
1/5	0.187650	–	0.169700	–	0.200110	–	0.191990	–
1/10	0.111190	0.76	0.115720	0.55	0.121310	0.72	0.121630	0.66
1/20	0.056829	0.97	0.073652	0.65	0.086137	0.49	0.091910	0.40
1/40	0.028911	0.98	0.045233	0.70	0.059927	0.52	0.067928	0.44
1/80	0.012443	1.22	0.023754	0.93	0.035052	0.77	0.047736	0.51
1/160	0.006982	0.83	0.015361	0.63	0.028422	0.30	0.036563	0.38

5 Conclusions and discussion

The high-resolution ENO-like schemes for the model (1) constructed in this work can approximate exact solutions very well for all kinds of data: supersonic, subsonic, or both. The ENO-like scheme corresponding to $k = 3$ still works well even in the resonant regime, where the exact solution containing

multiple waves associated with different characteristic fields propagates with the same shock speed. This scheme still maintains some valuable properties of the original one for hyperbolic systems of conservation laws: it is oscillatory and has high order accuracy. Numerical tests show that the scheme has a much better accuracy than the Godunov-type scheme and can approximate smooth stationary waves with a second-order accuracy. The ENO-like scheme corresponding to $k = 3$ works as good as the van Leer-type scheme. However, the ENO-like schemes for larger k may suffer oscillations.

Acknowledgment

We are very grateful to the reviewers for their very constructive comments and helpful suggestions.

References

[1] Ambroso, A., Chalons, C., Coquel, F. and Galié, T. *Relaxation and numerical approximation of a two-fluid two-pressure diphasic model,* Math. Mod. Numer. Anal., 43 (2009), 1063–1097.

[2] Ambroso, A., Chalons, C. and Raviart, P.-A. *A Godunov-type method for the seven-equation model of compressible two-phase flow,* Computers & Fluids, 54 (2012), 67–91.

[3] Audusse, E., Bouchut, F., Bristeau, M-O., Klein, R. and Perthame, B. *A fast and stable well-balanced scheme with hydrostatic reconstruction for shallow water flows,* SIAM J. Sci. Comput., 25 (2004), 2050–2065.

[4] Baudin, M., Coquel, F. and Tran, Q.-H. *A semi-implicit relaxation scheme for modeling two-phase flow in a pipeline,* SIAM J. Sci. Comput., 27 (2005), 914–936.

[5] Ben-Artzi, M. and Falcovitz, J. *An upwind second-order scheme for compressible duct flows,* SIAM J. Sci. and Stat. Comput., 7(2006), 744–768.

[6] Botchorishvili, R., Perthame, B. and Vasseur, A. *Equilibrium schemes for scalar conservation laws with stiff sources*, Math. Comput., 72 (2003), 131–157.

[7] Botchorishvili, R. and Pironneau, O. *Finite volume schemes with equilibrium type discretization of source terms for scalar conservation laws,* J. Comput. Phys., 187 (2003), 391–427.

[8] Castro, M.J., Chalons, C., Del Grosso, A. and Morales de Luna, T. *Lagrange-projection methods for shallow water equations with movable bottom and erosion-deposition processes* Num. Math.: Theory, Meth. Appl., 16(2023), 1087–1126.

[9] Castro, C.E., and Toro, E.F. *A Riemann solver and upwind methods for a two-phase flow model in non-conservative form,* Internat. J. Numer. Methods Fluids, 50 (2006), 275–307.

[10] Chalons, C., Del Grosso, A.and Toro, E.F. *Numerical approximation and uncertainty quantification for arterial blood flow models with viscoelasticity,* J. Comput. Phys., 457 (2022), 111071.

[11] Chinnayya, A., LeRoux, A.-Y. and Seguin, N. *A well-balanced numerical scheme for the approximation of the shallow water equations with topography: the resonance phenomenon,* Int. J. Finite Vol., 1(4), 2004, 1–33.

[12] Coquel, F., El Amine, K., Godlewski, E., Perthame, B. and P. Rascle, *A numerical method using upwind schemes for the resolution of two-phase flows,* J. Comput. Phys. 136 (1997), 272–288.

[13] Coquel, F., Hérard, J.-M., Saleh, K. and Seguin, N. *Two properties of two-velocity two-pressure models for two-phase flows,* Commun. Math. Sci. 12 (2014), 593–600.

[14] Coquel, F., Saleh, K. and Seguin, N. *A robust and entropy-satisfying numerical scheme for fluid flows in discontinuous nozzles,* Math. Mod. Meth. Appl. Sci., 24 (2014), 2043–2083.

[15] Cuong, D.H. and Thanh, M.D. *A Godunov-type scheme for the isentropic model of a fluid flow in a nozzle with variable cross-section,* Appl. Math. Comput., 256 (2015) 602–629.

[16] Cuong, D.H. and Thanh, M.D. *A high-resolution van Leer-type scheme for a model of fluid flows in a nozzle with variable cross-section,* J. Korean Math. Soc., Vol. 54 (1) (2017), 141–175.

[17] Cuong, D.H. and Thanh, M.D. *Computing algorithms in resonant regime for a two-phase flow model,* Taiwan. J. Math. Dec. (2023), 1135–1168

[18] Dal Maso, G., LeFloch, P.G. and Murat, F. *Definition and weak stability of nonconservative products,* J. Math. Pures Appl., 74 (1995), 483–548.

[19] Gallouët, T., Hérard, J.-M. and Seguin, N. *Numerical modeling of two-phase flows using the two-fluid two-pressure approach,* Math. Models Methods Appl. Sci., 14 (2004) 663–700.

[20] Goatin, P. *Macroscopic traffic flow modelling: from kinematic waves to autonomous vehicles,* Commun. Appl. Ind. Math., 14(1) (2023), 1–16.

[21] Goatin, P. and LeFloch, P.G. *The Riemann problem for a class of resonant nonlinear systems of balance laws*, Ann. Inst. H. Poincare Anal. NonLineaire, 21 (2004), 881–902.

[22] Greenberg, J.M. and Leroux, A.Y. *A well-balanced scheme for the numerical processing of source terms in hyperbolic equations,* SIAM J. Numer. Anal., 33 (1996) 1–16.

[23] Han, X. and Li, G. *Well-balanced finite difference WENO schemes for the Ripa model,* Comput. Fluid. 134-135 (2016), 1–10.

[24] Harten, A., Engquist, B., Osher, S. and Chakravarthy, S. *Uniformly high order essentially non- oscillatory schemes, III,* J. Comput. Phys., 71(1987), 231–303.

[25] Isaacson, E. and Temple, B. *Nonlinear resonance in systems of conservation laws,* SIAM J. Appl. Math., 52 (1992) 1260–1278.

[26] Isaacson, E. and Temple, B. *Convergence of the* 2×2 *Godunov method for a general resonant nonlinear balance law,* SIAM J. Appl. Math., 55 (1995) 625–640.

[27] Kröner, D., LeFloch, P.G. and Thanh, M.D. *The minimum entropy principle for fluid flows in a nozzle with discontinuous cross-section*, Math. Mod. Numer. Anal., 42 (2008), 425–442.

[28] Kröner, D. and Thanh, M.D. *Numerical solutions to compressible flows in a nozzle with variable cross-section*, SIAM J. Numer. Anal., 43 (2005), 796–824.

[29] LeFloch, P.G. and Thanh, M.D. The Riemann problem for fluid flows in a nozzle with discontinuous cross-section, Comm. Math. Sci., 1 (2003), 763–797.

[30] LeFloch, P.G. and Thanh, M.D. *A Godunov-type method for the shallow water equations with variable topography in the resonant regime,* J. Comput. Phys., 230 (2011), 7631–7660.

[31] LeFloch, P.G. and Thanh, M.D. *The Riemann problem in continuum physics,* Appl. Math. Sci., Springer, 2024.

[32] Marchesin, D. and Paes-Leme, P.J. *A Riemann problem in gas dynamics with bifurcation. Hyperbolic partial differential equations III*, Comput. Math. Appl. (Part A), 12 (1986) 433–455.

[33] Munkejord, S.T. *Comparison of Roe-type methods for solving the two-fluid model with and without pressure relaxation,* Computers & Fluids, 36 (2007), 1061–1080.

[34] Saurel, R. and Abgrall, R. *A multi-phase Godunov method for compressible multifluid and multiphase flows,* J. Comput. Phys., 150 (1999), 425–467.

[35] Schwendeman, D.W., Wahle, C.W. and Kapila, A.K. *The Riemann problem and a high-resolution Godunov method for a model of compressible two-phase flow,* J. Comput. Phys., 212 (2006), 490–526.

[36] Shen, H. *A class of ENO schemes with adaptive order for solving hyperbolic conservation laws,* Computers & Fluids, 266, (2023), 106050.

[37] Shu, C.W. *Essentially non-oscillatory and weighted essentially non-oscillatory schemes for hyperbolic conservation laws. In: Quarteroni A. (eds) Advanced Numerical Approximation of Nonlinear Hyperbolic Equations.* Lecture Notes in Mathematics, vol 1697, Springer, Berlin, Heidelberg (1998), 325–432.

[38] Thanh, M.D. The Riemann problem for a non-isentropic fluid in a nozzle with discontinuous cross-sectional area, SIAM J. Appl. Math., 69 (2009), 1501–1519.

[39] Thanh, M.D., Kröner, D. and C. Chalons, *A robust numerical method for approximating solutions of a model of two-phase flows and its properties*, Appl. Math. Comput., 219 (2012), 320–344.

[40] Thanh, M.D., Kröner, D. and N.T. Nam, *Numerical approximation for a Baer-Nunziato model of two-phase flows*, Appl. Numer. Math., 61 (2011), 702–721.

[41] Thanh, N.X., Thanh, M.D. and Cuong, D.H. *A well-balanced high-order scheme on van Leer-type for the shallow water equations with temperature gradient and variable bottom topography,* Adv. Comput. Math., 47 (2021) 1–53.

[42] Xu, C., Zhang, F., Dong, H. and Jiang, H. *Arbitrary high-order extended essentially non-oscillatory schemes for hyperbolic conservation laws,* Int. J. for Num. Meth. Fluids, 93(7) (2021), 2136–2154.